Catalysts **2015**, *5*, 671-689; doi:10.3390/catal5020671

OPEN ACCESS

catalysts

ISSN 2073-4344

www.mdpi.com/journal/catalysts

Article

Catalytic Oxidation of Propene over Pd Catalysts Supported on CeO_2, TiO_2, Al_2O_3 and *M*/Al_2O_3 Oxides (*M* = Ce, Ti, Fe, Mn)

Sonia Gil [1], Jesus Manuel Garcia-Vargas [1], Leonarda Francesca Liotta [2,*], Giuseppe Pantaleo [2], Mohamed Ousmane [1], Laurence Retailleau [1] and Anne Giroir-Fendler [1,*]

[1] Département Chimie-Biochimie, Université de Lyon, Lyon, F-69003, France, Université Lyon 1, Villeurbanne, F-69622, CNRS, UMR 5256, IRCELYON, 2 avenue Albert Einstein, Villeurbanne, F-69622, France; E-Mails: sonia.gil@ircelyon.univ-lyon1.fr (S.G.); jesus.vargas@ircelyon.univ-lyon1.fr (J.M.G.-V.); mohamad.ousmane@gmail.com (M.O.); laurence.retailleau-mevel@ircelyon.univ-lyon1.fr (L.R.)

[2] Istituto per Lo Studio dei Materiali Nanostrutturati (ISMN)-CNR, via Ugo La Malfa, 153, 90146 Palermo, Italy; E-Mail: pantaleo@pa.ismn.cnr.it

* Authors to whom correspondence should be addressed; E-Mails: liotta@pa.ismn.cnr.it (L.F.L.); anne.giroir-fendler@ircelyon.univ-lyon1.fr (A.G.-F.); Tel.: +39-0916809371 (L.F.L.); +33-472-431-586 (A.G.-F.); Fax: +39-091-6809399 (L.F.L.); +33-472-431-695 (A.G.-F.).

Academic Editor: Jean-François Lamonier

Received: 2 March 2015 / Accepted: 9 April 2015 / Published: 22 April 2015

Abstract: In the following work, the catalytic behavior of Pd catalysts prepared using different oxides as support (Al_2O_3, CeO_2 and TiO_2) in the catalytic combustion of propene, in low concentration in excess of oxygen, to mimic the conditions of catalytic decomposition of a volatile organic compound of hydrocarbon-type is reported. In addition, the influence of different promoters (Ce, Ti, Fe and Mn) when added to a Pd/Al_2O_3 catalyst was analyzed. Catalysts were prepared by the impregnation method and were characterized by ICP-OES, N_2 adsorption, temperature-programmed reduction, temperature-programmed oxidation, X-ray diffraction, X-ray photoelectron spectroscopy and transmission electron microscopy. Catalyst prepared using CeO_2 as the support was less easily reducible, due to the stabilization effect of CeO_2 over the palladium oxides. Small PdO particles and, therefore, high Pd dispersion were observed for all of the catalysts, as confirmed by XRD and TEM. The addition of Ce to the Pd/Al_2O_3 catalysts increased the metal-support interaction and the formation of highly-dispersed Pd species. The addition of Ce and Fe improved the catalytic behavior of the Pd/Al_2O_3 catalyst;

however, the addition of Mn and Ti decreased the catalytic activity in the propene oxidation. Pd/TiO_2 showed the highest catalytic activity, probably due to the high capacity of this catalyst to reoxidize Pd into PdO, as has been found in the temperature-programmed oxidation (TPO) experiments.

Keywords: Pd-doped supported catalysts; CeO_2; TiO_2; Al_2O_3 and *M*/Al_2O_3 oxides; propene oxidation

1. Introduction

One of the major challenges of today is the environmental problem associated with the atmospheric emissions of pollutants after the combustion of fossil fuels. In this way, volatile organic compounds (VOCs) represent a serious environmental problem, because of their direct (carcinogenic or mutagen) and indirect effects (ozone and smog precursors) on the environment and health [1–3]. Several different compounds are usually included in the VOC group, such as aromatic and aliphatic hydrocarbons, alcohols, ketones and aldehydes; compounds that share ease in being oxidized. Therefore, catalytic oxidation of VOCs is an interesting technique in order to reduce the emissions of pollutants during the fossil fuel combustion process, as the low concentration of VOCs in most of the cases does not allow direct combustion [4–6]. Propene is among the most investigated probe molecules in the field of VOC catalytic oxidation, because alkenes are among the major families in automotive exhausts and because of its high photochemical ozone creativity potential (POCP) [7].

Noble metals are often selected as the active phase in most of the VOC catalytic oxidation studies, despite its high price, low thermal stability and tendency of poisoning due to the superior catalytic activity of these species compared to non-noble metals [8]. Most of the catalysts employed in the catalytic oxidation of VOCs are based on the noble metal system, but the development of fuels with a lower quantity of lead, one of the major poisons in palladium catalytic systems [9], has also increased the interest in using Pd as the active phase, due to its lower price compared to other noble metals [10] and its high catalytic activity.

One of the key parameters when developing a catalyst is the nature of the support, as it is well-known that it plays an important role in improving the activity and durability of supported noble metals, with great importance of the surface properties and the metal-support interaction. The catalytic behavior of Pd-supported catalysts in catalytic oxidation strongly depends on the acid-base properties of the support [11,12], as well as on the metal-support interaction [13,14]. The metal-support interaction plays an important role in the oxidation state of Pd during the oxidation of VOCs, as reducible oxides, like TiO_2, CeO_2, Nb_2O_5 and La_2O_3, favor the oxidation of Pd into PdO, while non-reducible oxides do not [15,16]. Pd/Al_2O_3 catalyst has been studied in the combustion of hydrocarbons by several authors [17–20], showing high catalytic activity despite having different catalytic behavior depending on the hydrocarbon [18]. The addition of reducible oxides (CeO_2, TiO_2, *etc*.) can modify the reduction behavior of the catalyst, so it is interesting to check the influence of these oxides in the oxidation state of Pd and, therefore, in the catalytic activity of the system Pd/Al_2O_3.

In the present study, the catalytic oxidation of propene was investigated over Pd catalysts supported over CeO_2, TiO_2, Al_2O_3 and M/Al_2O_3 oxides (M = Ce, Ti, Fe, Mn). The experimental conditions for the catalytic tests, low concentration of propene (1,000 ppm) in excess of oxygen 9 vol%, were chosen to mimic the conditions of catalytic decomposition of a volatile organic compound of the hydrocarbon-type [2].

The synthesized catalysts were characterized by ICP-OES (inductively-coupled plasma optical emission spectroscopy), specific surface area measurements through the BET method, TPR (temperature-programmed reduction), TPO (temperature-programmed oxidation), XRD (X-ray diffraction), XPS (X-ray photoelectron spectroscopy) and TEM (transmission electron microscopy), in order to evaluate the influence of the different supports and the metal doped on the catalytic properties. Attention was also focused on the catalyst stability during three consecutive cycles.

2. Results and Discussion

2.1. Support and Catalysts Characterization

The physicochemical properties of the commercial supports, Al_2O_3, TiO_2 and CeO_2, and doped-Al_2O_3 supports are listed in Table 1. N_2 adsorption-desorption isotherms, pore size distributions and pore volumes of the commercial supports, Al_2O_3, TiO_2 and CeO_2, are presented in Figure 1. All commercial supports present a N_2 adsorption/desorption profile (Figure 1a) that can be assigned to the Type IV isotherm, showing a hysteresis loop due to capillary condensation representative of a mesoporous material. The three commercial supports, TiO_2, CeO_2 and Al_2O_3, of a mesoporous nature, had BET surface areas ranging from ~80–160 $m^2 \cdot g^{-1}$ and total pore volumes equal to 0.3, 0.4 and 0.2 cm^3/g, respectively. The pore size distribution (Figure 1b) showed a narrow peak centered at 4.6 nm for the Al_2O_3; a broader peak distribution centered at 8.1 nm was observed for TiO_2, while a very low and large distribution curve ranging from around 15 to 50 nm was found for the CeO_2 support. After doping of alumina support (5 mol% of Ce, Ti, Fe and Mn) and calcining at 500 °C, the shape of the N_2 isotherms remained almost the same as that of the commercial alumina (not shown). The values of BET surface areas associated with the doped-alumina (Table 1) were generally lower than the commercial one, except for Ti/Al_2O_3, showing almost the same BET surface area as alumina. It is likely that a partial blockage of the pores of the material occurs upon deposition of the metal precursor and calcination at 500 °C 3 h. Accordingly, the mean pore diameter shifted to slightly higher values, suggesting filling of the small pores. However, the total pore volumes being constant at 0.2 cm^3/g, it could be speculated that the metal doping was largely on the external surface of the alumina.

After the Pd introduction, the shape of the N_2 isotherms remained almost the same as those of the supports (not shown); however, the specific surface area values were lower (Table 2). This finding could suggest a partial blockage of the porous structure of materials upon Pd deposition and further calcination at 400 °C 4 h. The thermal stability of the doped-alumina supports and Pd catalysts was studied after three tests of propene oxidation (APT: after propene tests), see Tables 1 and 2). The specific surface of the doped-alumina and the Pd catalysts slightly decreased (~10 $m^2 \cdot g^{-1}$), which means that the properties of both doped-alumina and Pd catalysts were not seriously modified after the heat treatment [21].

Table 1. Physicochemical properties of the supports.

Supports	BET surface area ($m^2 \cdot g^{-1}$)	BET surface area APT[1] ($m^2 \cdot g^{-1}$)	Total pore volume ($cm^3 \cdot g^{-1}$)	Mean pore diameter (nm) [2]
TiO_2	115	-	0.3	8.1
CeO_2	79	-	0.4	15.0–50.0 (broad curve)
Al_2O_3	157	-	0.2	4.6
Ce/Al_2O_3	140	128	0.2	5.0
Ti/Al_2O_3	155	150	0.2	4.5
Fe/Al_2O_3	145	143	0.2	5.0
Mn/Al_2O_3	146	145	0.2	5.0

[1] Used after propene tests (APT). [2] Calculated by the BJH method.

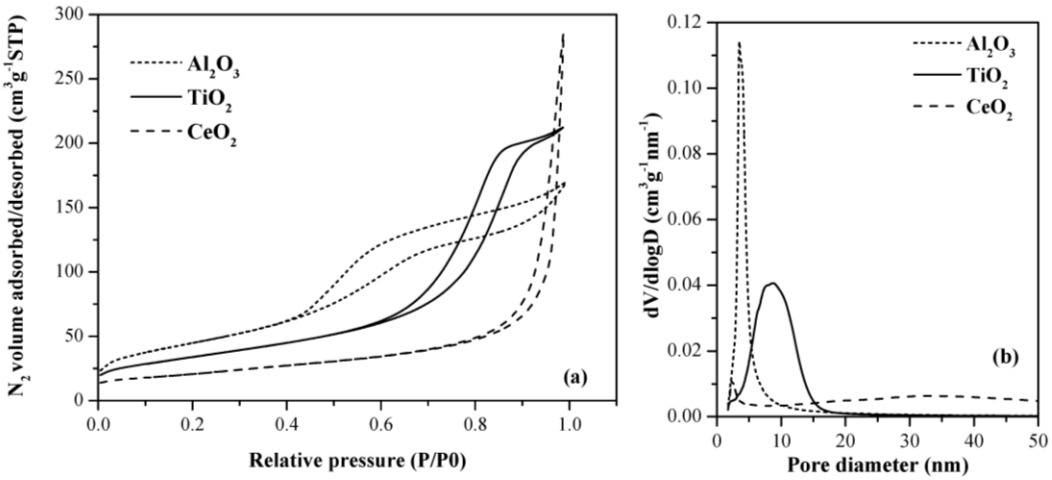

Figure 1. (**a**) N_2 adsorption/desorption isotherms and (**b**) pore size distributions associated with CeO_2, Al_2O_3 and TiO_2 supports.

Table 2. Physicochemical properties of the Pd supported catalysts.

Catalysts	BET surface area ($m^2 \cdot g^{-1}$)	BET surface area APT[1] ($m^2 \cdot g^{-1}$)	Pd loading (wt%) [2]	$dCeO_2$ (nm) [3]	*p*-Value [4]
Pd/TiO_2	102	99	0.8	-	0.64
Pd/CeO_2	77	77	0.5	105	0.86
Pd/Al_2O_3	148	144	0.8	-	1.04
$Pd/Ce/Al_2O_3$	137	132	0.8	13	-
$Pd/Ti/Al_2O_3$	154	142	0.8	-	-
$Pd/Fe/Al_2O_3$	138	130	0.8	-	-
$Pd/Mn/Al_2O_3$	135	138	0.8	-	-

[1] Used after propene tests (APT). [2] Pd (wt%) analytical loading determined by ICP-OES. [3] Average CeO_2 crystal sizes determined by XRD for the half-width of the main CeO_2 peaks corresponding to the (111) reflection. [4] The ratio between the area of the PdO decomposition peaks and the area of the reoxidation peaks, temperature-programmed oxidation (TPO) analysis.

The results obtained in the X-ray diffraction experiments are plotted in Figure 2. The main diffraction peaks corresponding to the support can be observed for the Pd/Al_2O_3, Pd/TiO_2 and Pd/CeO_2 catalysts (Figure 2a), while peaks corresponding to PdO were only obtained for the Pd/Al_2O_3 catalyst, with a small and broad peak obtained at a 2θ value of 33.9°, which corresponds to the diffraction peak of Miller indices (101). The peaks obtained for the supports correspond to the main diffraction peaks of γ-Al_2O_3, the main diffraction peaks of TiO_2 (brookite) and the typical diffraction peaks related to the cubic lattice of pure CeO_2 (CaF_2 structural type) [22], for the Pd/Al_2O_3, Pd/TiO_2 and Pd/CeO_2 catalysts, respectively. Comparing diffraction profiles obtained for the promoted Al_2O_3-supported catalysts, the main diffraction peaks are due to the γ-Al_2O_3 phase. Only $Pd/Ce/Al_2O_3$ and $Pd/Fe/Al_2O_3$ showed diffraction peaks attributed to CeO_2 and Fe_2O_3 phases, with higher intensity of ceria features suggesting higher crystallinity. The presence of the main diffraction peak corresponding to PdO can be observed in $Pd/Ti/Al_2O_3$ and $Pd/Mn/Al_2O_3$, while for the other two catalysts, it is not very clear, probably due to the overlap of other diffraction peaks and/or the high dispersion of the PdO particles in these catalysts. It should be remarked that the main diffraction peak of PdO, when present, was very small and broad, which indicates a high dispersion of this metal for all of the catalysts. Moreover, in order to better understand the differences in the catalytic behavior of Pd/CeO_2 and $Pd/Ce/Al_2O_3$, the crystal size of CeO_2 was determined in these two catalysts by using the Debye–Scherrer equation, using the data from the XRD patterns ((111) reflection of CeO_2). The data obtained are shown in Table 2, where a much lower value of CeO_2 crystal size was found for the catalyst $Pd/Ce/Al_2O_3$ (13 nm ± 1.3) compared to that obtained for Pd/CeO_2 (105 nm ± 10.5).

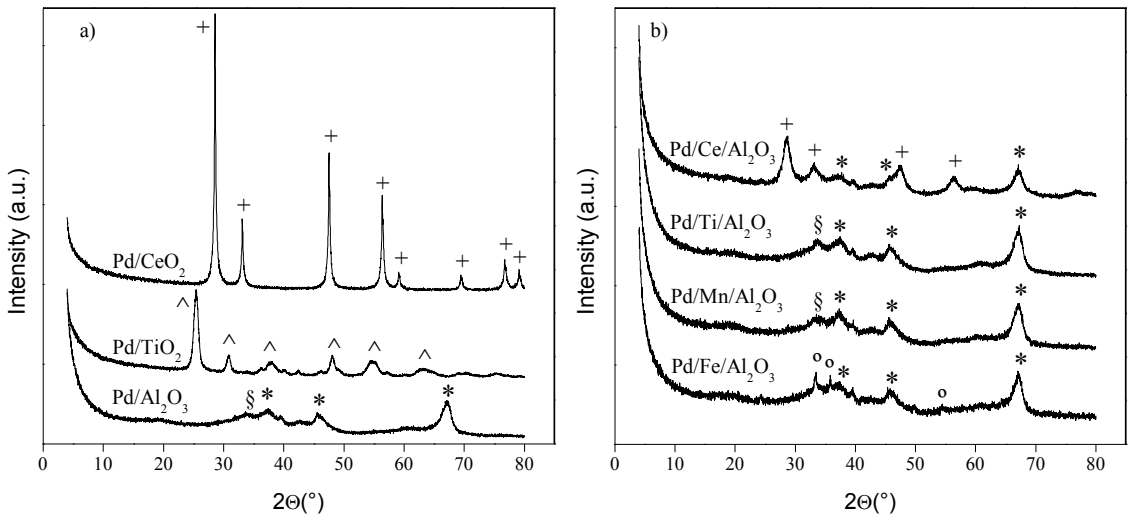

Figure 2. XRD profiles of (**a**) Pd-supported catalysts and (**b**) Pd-doped-supported catalysts, where § denotes reflection of PdO, * denotes reflection of γ-Al_2O_3, + denotes reflection of CeO_2, ^ denotes reflection of TiO_2 and ° denotes reflection of Fe_2O_3.

In order to investigate the behavior of Pd-supported catalysts under oxidative conditions, TPO heating/cooling ramps were carried out (Figure 3). During the heating ramp, a positive peak at around 450 °C was observed for Pd/TiO_2 and for Pd/CeO_2 that could be attributed to the decomposition of adsorption oxygen species [23], whereas the positive peak in the range of 750–850 °C could be ascribed to the PdO decomposition [23–25]. The obtained results showed that the PdO decomposition

occurred over CeO_2 at higher temperatures than over TiO_2 and Al_2O_3, suggesting for Pd/CeO_2 the strongest interaction between the PdO species and the support [24,25]. During the cooling ramp, a single negative peak at 558, 637 and 720 °C, corresponding to the O_2-consumption, was observed for the Pd/Al_2O_3, Pd/TiO_2 and Pd/CeO_2 catalysts, respectively. This negative peak corresponds to the reoxidation of metallic Pd to PdO [23], and the temperature strongly depends on the support. The finding of such a high reoxidation temperature, 720 °C, for Pd/CeO_2 suggests a very high reoxidation tendency of metallic palladium to PdO over ceria. Taking into account the ratio between the area of the PdO decomposition peak and the area of the reoxidation peak, the *p*-value was calculated [24] and reported in Table 2. The smaller the *p*-value, the higher is the reoxidation ability of Pd into PdO. A very low *p*-value was detected for Pd/TiO_2.

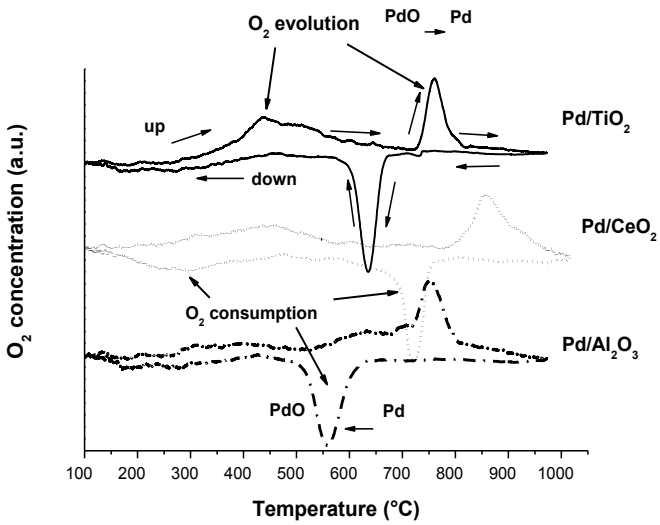

Figure 3. TPO profiles of Pd-supported catalysts.

During the cooling ramp, for the Pd/CeO_2 catalyst, an oxygen consumption peak occurred also at low temperature, at around 350 °C, which could be associated with the reoxidation of the CeO_2 surface partially reduced during the high-temperature heating step.

In Figure 4a, TPR curves of catalysts Pd/CeO_2, Pd/TiO_2 and Pd/Al_2O_3, are displayed. Peaks corresponding to different types of PdO species were observed at different temperatures depending on the support. Very small PdO particles (easily reducible, peak at −45 °C) were detected over TiO_2. A second peak appearing at 8 °C, also found for Pd/Al_2O_3, was attributed to the reduction of bulky PdO particles [26]. For both catalysts, Pd/TiO_2 and Pd/Al_2O_3, decomposition of β-hydride species takes place at 60 °C (negative peak). Such species are formed through hydrogen adsorption/diffusion in the Pd° crystallites [27]. Over CeO_2, which is known to stabilize PdO, reduction occurred at a higher temperature (25 °C). Moreover, a second peak, at 50 °C, ascribed to the reduction of the ceria surface in contact with palladium, was also found. Above 300 °C, CeO_2 and TiO_2 were reduced (surface reduction at around 400–500 °C, bulk reduction above 700 °C). Figure 4b, shows the reduction profile of the alumina-doped catalysts. In the $Pd/Ti/Al_2O_3$ catalyst, the peak corresponding to the reduction of PdO around 0 °C is much less pronounced than that observed for Pd/TiO_2 or Pd/Al_2O_3, and the decomposition of β-hydride shows two different peaks, probably due to the different interaction of PdH with TiO_2 and Al_2O_3. $Pd/Ce/Al_2O_3$ showed two main reduction peaks for PdO at 11 °C and 40 °C,

the first one probably due to the interaction of PdO with Al_2O_3 and the other to the interaction with CeO_2. No clear reduction peak of PdO species was found for the Pd/Fe/Al_2O_3 catalyst, which is probably due to the reduction of this oxide during the stabilization of the signal due to the easiness of this process in this catalyst. Reduction of PdO takes place at 19 °C for the Pd/Mn/Al_2O_3 catalyst, followed by the decomposition of PdH and one big reduction peak at 140 °C, assigned to the reduction of manganese oxides [28].

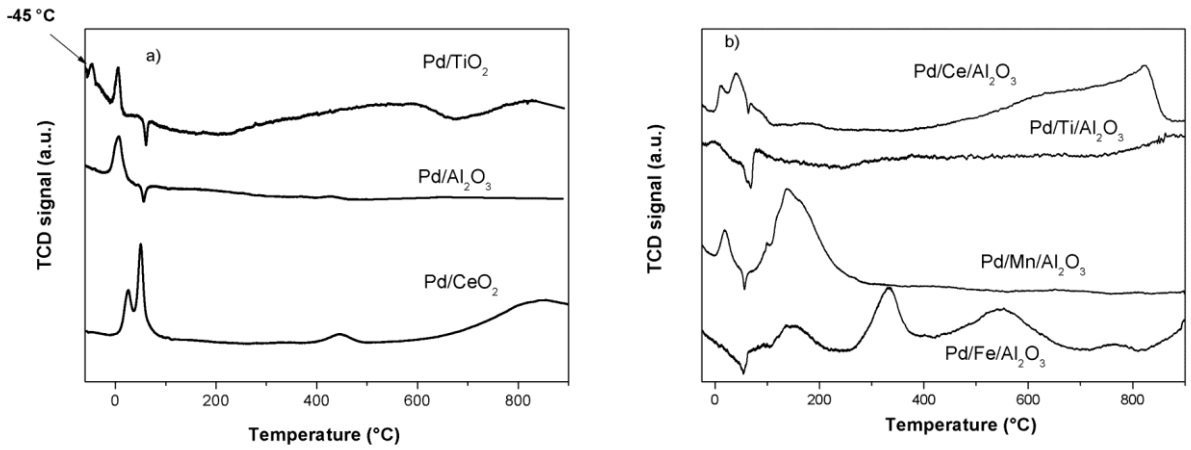

Figure 4. Temperature-programmed reduction (TPR) curves of (**a**) Pd-supported catalysts and (**b**) Pd-doped-supported catalysts.

Figure 5 shows the HR-TEM images of the Pd-supported catalyst and Pd-doped-supported catalysts. All catalysts exhibited small and well-dispersed PdO_x particles with surface area-weighted PdO_x diameters between 4–10 nm ± 1.

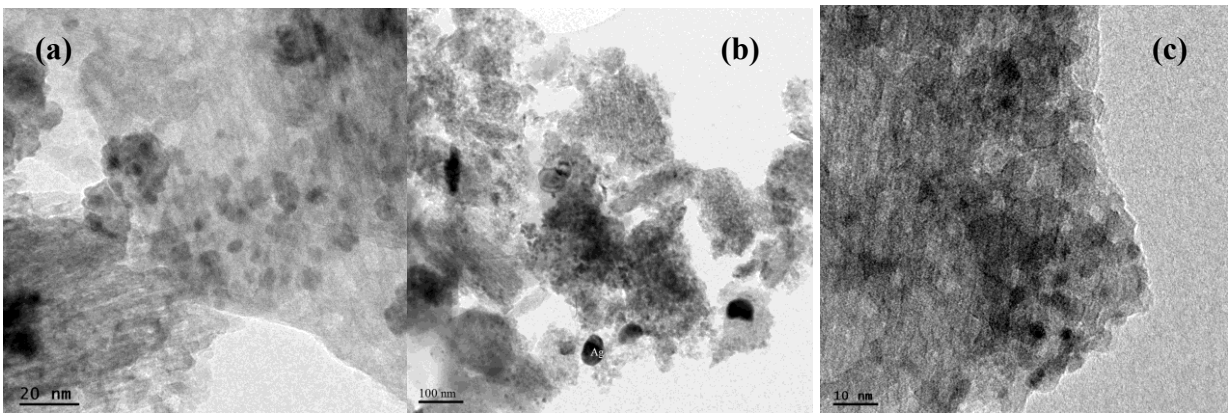

Figure 5. *Cont.*

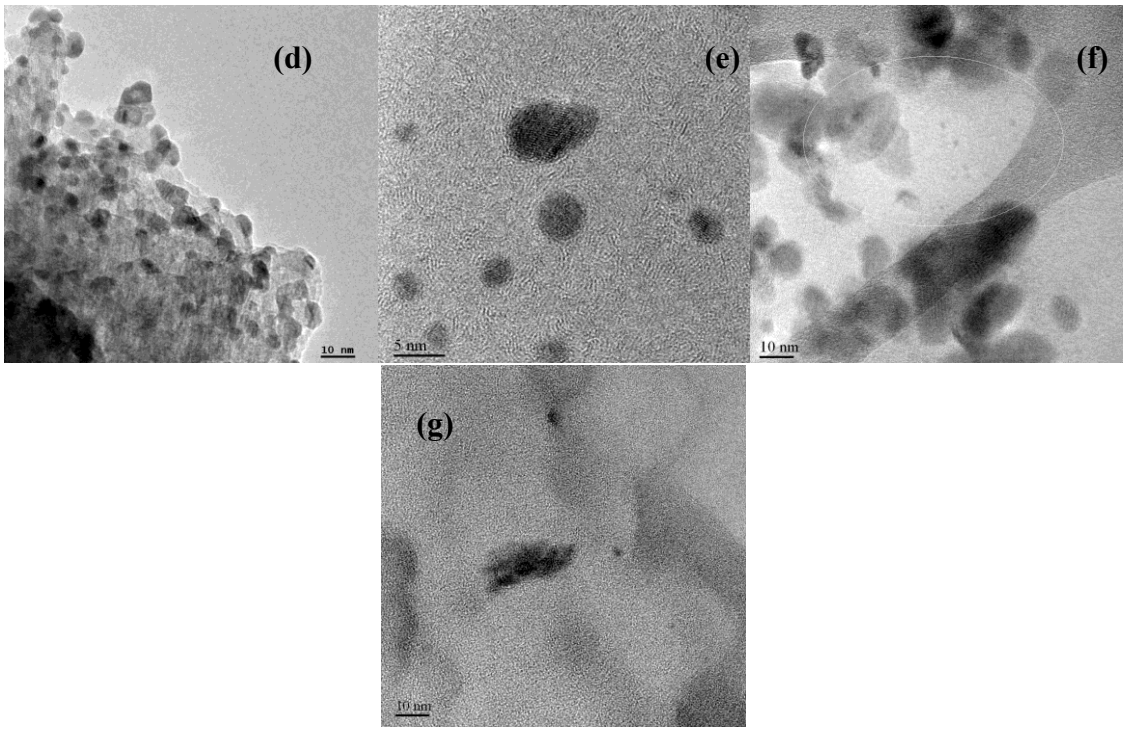

Figure 5. HR-TEM images of the Pd-supported catalysts: (**a**) Pd/Al_2O_3; (**b**) $Pd/Ce/Al_2O_3$; (**c**) $Pd/Fe/Al_2O_3$; (**d**) $Pd/Mn/Al_2O_3$; (**e**) $Pd/Ti/Al_2O_3$; (**f**) Pd/TiO_2; and (**g**) Pd/CeO_2.

The chemical state and the chemical surface composition of the Pd-supported catalysts were evaluated by XPS analyses. The binding energies (BEs) and the atomic ratios are presented in Table 3. XPS profiles of the Al 2p for the Pd/Al_2O_3 and $Pd/M/Al_2O_3$ catalysts are shown in Figure 6. The peaks are centered in the range of 74–74.4 eV, for all Al_2O_3-catalysts, corresponding to the γ-Al_2O_3, in accordance with the XRD results, which mean that the BE of the alumina was not modified after being metal doped. The O/Al atomic ratio showed for the metal-doped catalysts an increased amount of oxygen on the surface. The M/Al atomic ratio changed in the following order: $Pd/Ce/Al_2O_3$ < $Pd/Mn/Al_2O_3$ < $Pd/Ti/Al_2O_3$ < $Pd/Fe/Al_2O_3$; suggesting that among the series of metal-doped catalysts, the highest dispersion on the alumina surface occurred for Fe species.

Table 3. Binding energies (BEs) and atomic ratios obtained from XPS analyses.

Catalysts	Binding Energies (eV)										Atomic Surface Ratio	
	Al 2p	[1] Pd $3d_{5/2}$. Bulk PdO	[1] Pd $3d_{5/2}$. PdO_2	O 1s	Ti $2p_{3/2}$	Ce $3d_{5/2}$	[2] Ce^{4+}	[2] Ce^{3+}	Fe $2p_{3/2}$	Mn $2p_{3/2}$	O/Al	M/Al
Pd/TiO_2	-	336.1 (100)	-	529.7	458.4	-	-	-	-	-	-	
Pd/CeO_2	-	-	337.4 (100)	529.1	-	881.9	83	17	-	-	-	
Pd/Al_2O_3	74.1	336.4 (100)	-	530.8	-	-	-	-	-	-	1.66	
$Pd/Ce/Al_2O_3$	74.2	336.1 (83.2)	338.1 (16.4)	530.9	-	882.1	69	31	-	-	1.92	0.025
$Pd/Ti/Al_2O_3$	74	336.3 (100)	-	530.8	458.5	-	-	-	-	-	1.79	0.052
$Pd/Fe/Al_2O_3$	74	336.1 (100)	-	530.5	-	-	-	-	710	-	1.90	0.09
$Pd/Mn/Al_2O_3$	74	336.7 (100)	-	530.9	-	-	-	-	-	641.9	1.74	0.04

[1] The value in parentheses represents the atomic percentages of the palladium chemical components. [2] The percentages of the chemical states of cerium (Ce^{3+} and Ce^{4+}) on the surface.

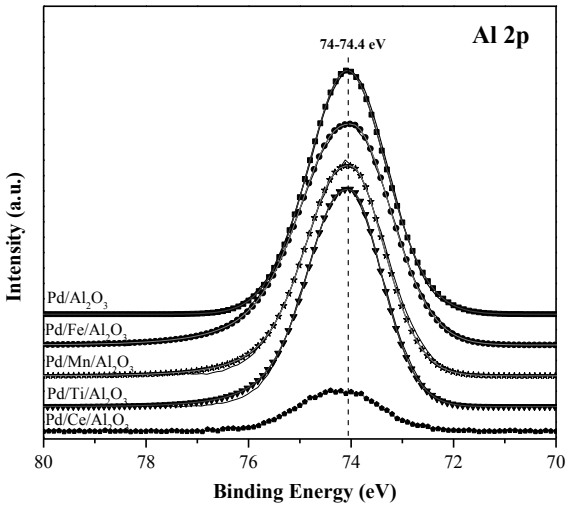

Figure 6. Al 2p XPS spectra of Pd/Al_2O_3 and Pd-doped-Al_2O_3 catalysts.

Figure 7 shows the chemical state of palladium for all catalysts. The Pd 3d spectra of the Pd/Al_2O_3, $Pd/M/Al_2O_3$ and Pd/TiO_2 catalysts (Figure 7) was characterized by the Pd $3d_{5/2}$ peak at 336.1 ± 0.6 eV, corresponding to the Pd^{2+} (bulk PdO) [12,29–31], whereas the Pd/CeO_2 catalyst presented the Pd $3d_{5/2}$ binding energy at 337.4 eV. This peak has been associated by Anna MariaVenezia *et al.* and Yushui Bi *et al.* with Pd^{4+}, as in PdO_2, due to the oxygen incorporation into the PdO crystal lattice during calcinations [12,32].

Moreover, XPS profiles of the $Pd/Ce/Al_2O_3$ catalyst showed that the oxidized palladium was presented in two chemical states, bulk PdO at 336.1 eV and highly-dispersed and deficiently-coordinated Pd^{2+} in contact with the support to form palladium-aluminate structures at 338.1 eV [31] or PdO_2 [12,32], inducing the formation of new interfacial sites for the oxidation reaction. The percentage of the chemical states of palladium is presented in Table 3. The coexistence of these two oxidation states of palladium and/or the formation of palladium-aluminate structures suggests a greater Pd/Ce/support interaction, as has been described by several authors [31,33]. This Pd-Ce interaction could be promoted by ceria species in the reduced state (Ce^{3+}) presented in this catalyst (Table 3) [33]. Moreover, the presence of the Ce^{3+} species results in greater oxygen vacancies due to the formation of a defective ceria structure, as has been reported in previous articles [34]. The increase of the lattice oxygen was related to high metal-particle nucleation sites. Thus, the Ce incorporation on the $Pd/M/Al_2O_3$-supported catalyst structure favors the formation of highly-dispersed and deficient Pd^{2+}, increasing the metal-support interaction and the stabilization of metal particle deposition. Figure 8a shows the Ce 3d spectra of the Pd/CeO_2 and $Pd/Ce/Al_2O_3$ catalysts, where both catalyst presented the same characteristic peaks of pure CeO_2, according to the convention established by Burroughs [35,36]. Thus, peaks 1, 3, 4, 5 and 6, 8, 9, 10 refer to $3d_{3/2}$ and $3d_{5/2}$ binding energies, respectively, and are characteristic of Ce^{4+} states, whereas peaks 2 and 7 refer to $3d_{3/2}$ and $3d_{5/2}$, respectively, and are attributed to the Ce^{3+} states. Moreover, The Ti 2p spectra of the Pd/TiO_2 and $Pd/Ti/Al_2O_3$ are shown in Figure 8b. The Ti $2p_{3/2}$ peak of both catalysts was centered at 458.4–458.5 eV, corresponding to the Ti^{4+} species (TiO_2), in accordance with the XRD results. In addition, according to Figure 8c,d, the binding energies of the Fe $2p_{3/2}$ (710 eV) and Mn-doped $2p_{3/2}$ (641.9 eV) could be ascribed to the Fe^{3+} (Fe_2O_3) and Mn^{4+} (MnO_2) [37,38].

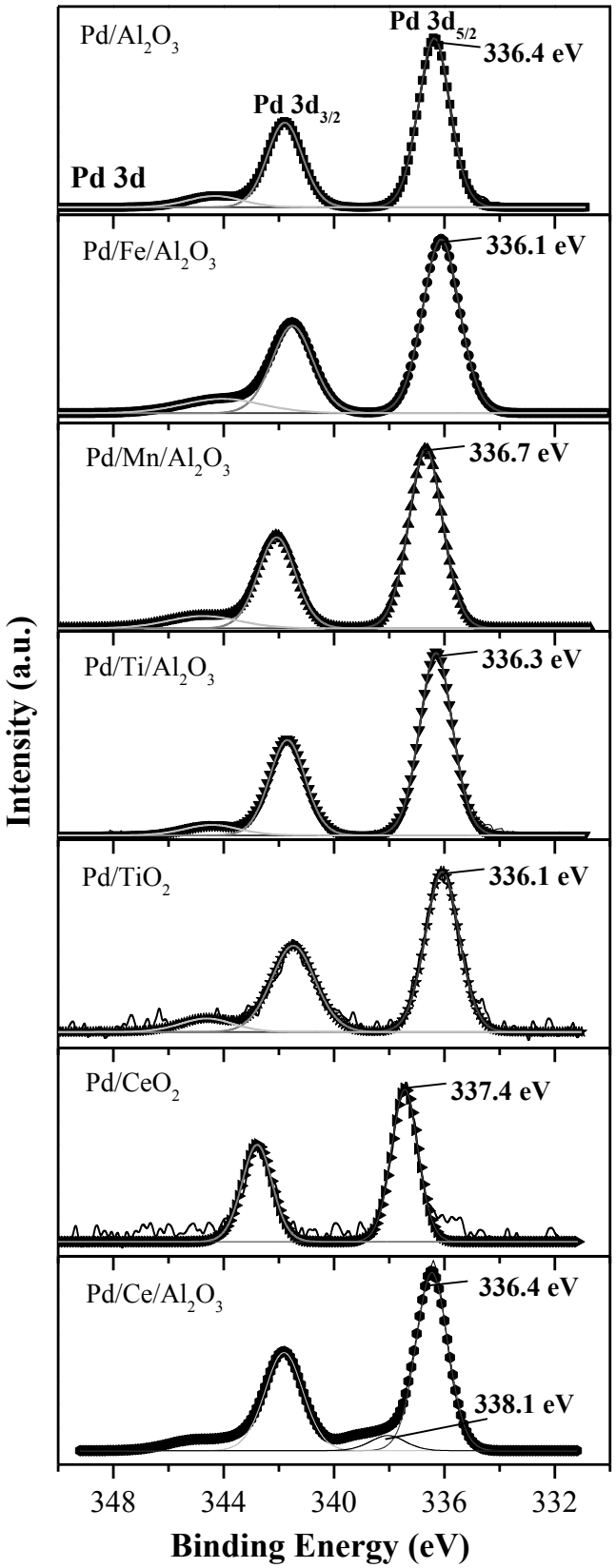

Figure 7. Pd 3d XPS spectra of Pd-supported catalysts.

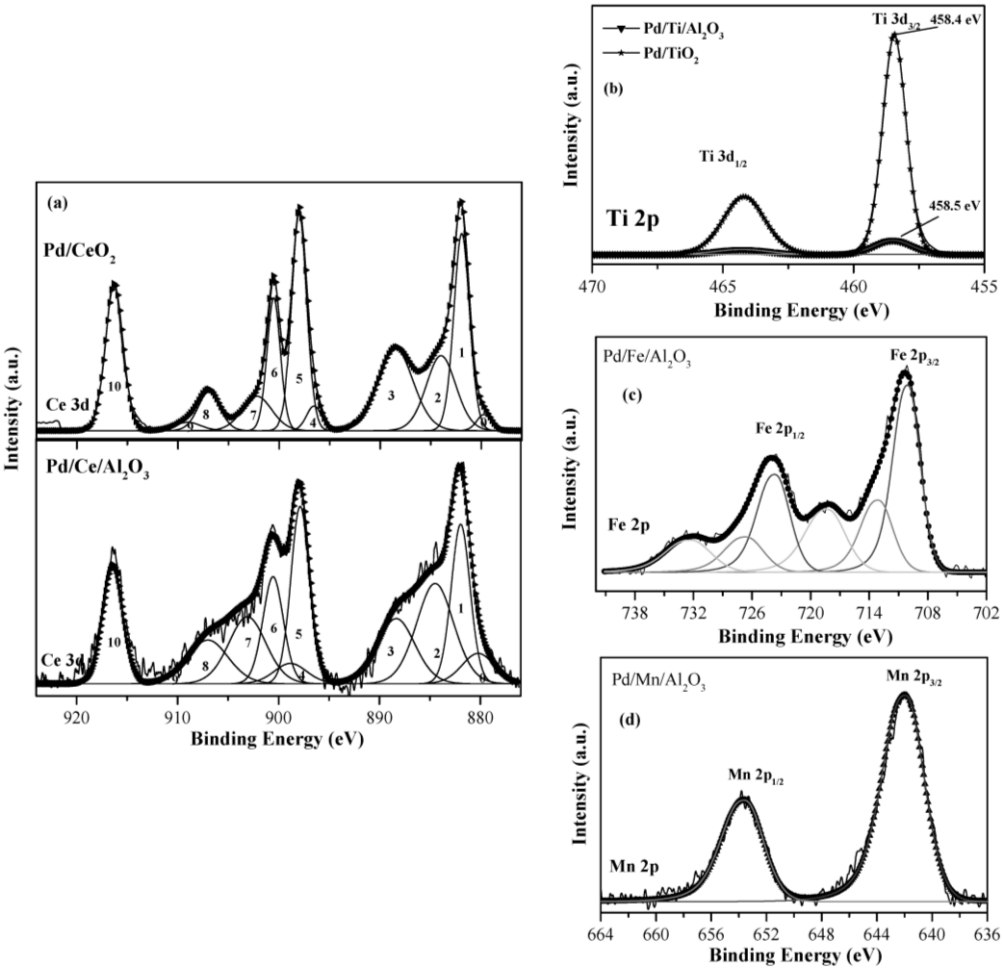

Figure 8. XPS spectra of Pd-supported catalysts: (**a**) Ti 2p; (**b**) Ce 3d; (**c**) Fe 2p; and (**d**) Mn 2p.

2.2. Catalytic Tests: Oxidation of Propene

The above characterized catalysts based on Pd supported on Al_2O_3, TiO_2 and CeO_2 were tested in the propene oxidation. The catalytic oxidation of propene was investigated in a tubular fixed-bed reactor under a reactive gas mixture containing 1000 ppm of C_3H_6 and 9 vol% O_2 in He at a gas hourly space velocity (GHSV) of 35,000 h^{-1}. Figure 9 shows the catalytic activity in terms of propene conversion as a function of the temperature (light-off curve) during the cooling ramp. The following sequence in activity was detected: Pd/TiO_2 > Pd/Al_2O_3 > Pd/CeO_2; suggesting that the nature of the support strongly influences the activity.

In order to evaluate the real effect of the support and alumina doping, the catalytic results were expressed as specific reaction rates calculated at 135 °C (mmolC_3H_6 s^{-1} mol_{Pd}^{-1}), Figure 10. The same catalytic trend was obtained, where Pd/TiO_2 was the most active, Pd/CeO_2 was the worst sample and Pd alumina-based catalysts showed an intermediate activity. This suggests that the support also plays an important role in the catalytic activity and stability of the Pd catalysts. Thus, the support used has a strong influence on the oxidation state of the active phase, as has been confirmed by XPS. Therefore, the higher catalytic activity of the Pd/TiO_2 and Pd/Al_2O_3 catalysts could be attributed to the Pd^{2+} species detected in these catalysts, while for the case of Pd/CeO_2 catalyst, the presence of Pd^{4+} species could be responsible for its low catalytic activity. Moreover, the higher activity of Pd/TiO_2 could be

attributed to the higher ability of this catalyst to reoxidize the metallic Pd into PdO, as has been corroborated by TPO from the parameter *p*-value (Table 2), according to the redox properties of this catalyst and the oxygen mobility [12,39].

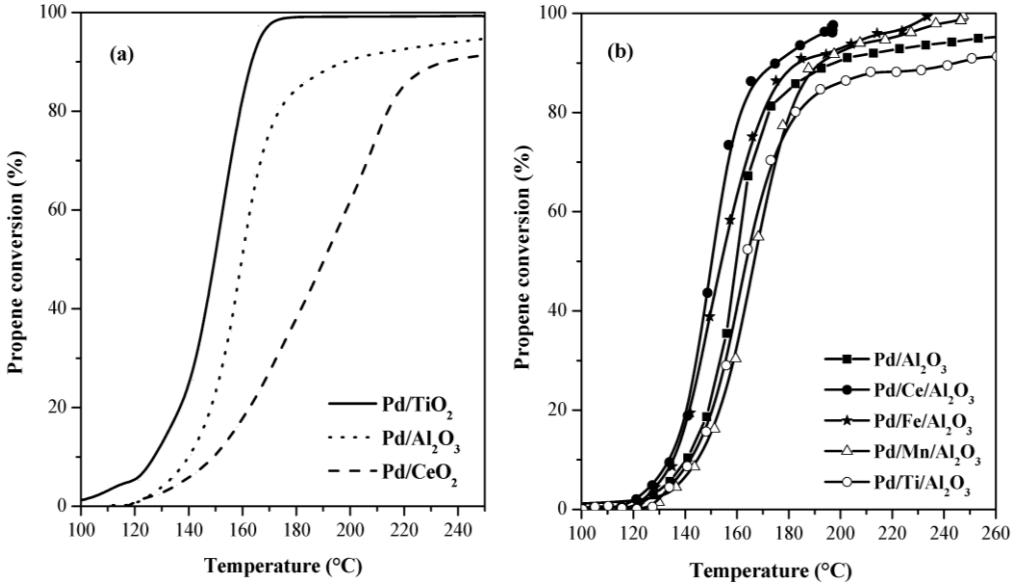

Figure 9. C_3H_6 conversion (%) *versus* temperature (light-off curve) of (**a**) Pd-supported catalysts and (**b**) Pd-doped-supported catalysts, during the cooling ramp.

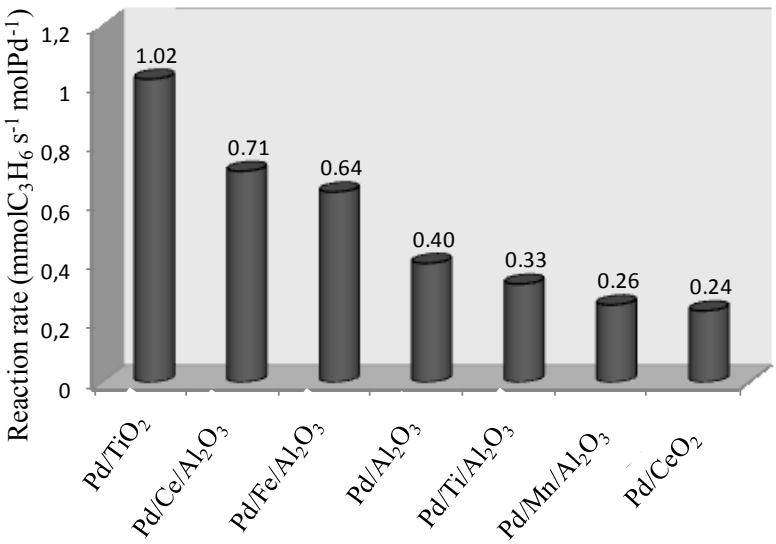

Figure 10. Catalytic activity of Pd-supported catalysts as specific reaction rates calculated at 135 °C.

In addition, the obtained results showed that the addition of Ce and Fe improves the catalytic activity of Pd/doped-alumina catalysts, while no positive effect was played by doping of Ti and Mn; Figures 9b and 10. Several factors may contribute to the observed catalytic trend, such as the dispersion of the metal dopant over the alumina, as well as the amount of available oxygen on the catalyst surface. Accordingly, $Pd/Fe/Al_2O_3$, exhibiting quite appreciable activity, was characterized by

the highest M/Al surface atomic ratio and quite a high O/Al value. On the other hand, it is likely that other factors influence the activity; indeed, the Pd/Ce/Al_2O_3 catalyst with a very low Ce amount on the surface was the most active Pd-doped-Al_2O_3-supported catalysts. This finding could be attributed to the small CeO_2 crystallites formed in this catalyst and the formation of the highly-dispersed and deficiently-coordinated Pd^{2+} in contact with the support, which favors the higher Pd/Ce/support interaction, as has been observed by XPS and XRD analyses, inducing the formation of new interfacial sites for the oxidation reaction [31].

In other words, the high catalytic activity of the Pd/Ce/Al_2O_3 catalyst could be related to the high Pd/Ce/Al_2O_3 interaction, generated by the increased oxygen vacancy (defects), which promoted the palladium oxide stabilization and more active sites for the oxidation reaction [31,34]. Moreover, Pd/CeO_2 catalyst was less active than the Pd/Ce/Al_2O_3 according to the higher CeO_2 crystallite size and lower surface area [2,31].

In addition, the catalyst stability was evaluated by performing three consecutive catalytic runs for each catalyst. Table 4 lists the temperatures corresponding to 20% (T_{20}), 50% (T_{50}) and 80% (T_{80}) of propene conversion. No appreciable catalytic deactivation was detected after three consecutive catalytic runs, where the different temperatures are close (±10 °C).

Finally, the apparent activation energies were determined for the different Pd-supported catalysts, where the integration equation of first order with respect to propene was used to calculate the reaction rate constants k. The corresponding Arrhenius plots (not shown) were linear for conversion values between 10% and 80%, excluding the occurrence of diffusion limitation. In Table 5, the apparent activation energies E_{act} along with the pre-exponential factor A of the Arrhenius equation, $k = A\ e^{(-Eact/RT)}$, are listed. The calculated activation energies and the pre-exponential factors are comparable with values previously reported for propene oxidation [40–42]. Differences in the activation energies and pre-exponential factors, A, reflect different active site ensembles in the catalysts, as a function of the support.

Table 4. Catalytic performances of the Pd-supported catalysts on the propene oxidation during the cooling ramp (third catalytic run).

Catalysts	T_{20} (°C) [1]			T_{50} (°C) [1]			T_{80} (°C) [1]		
	I run	II run	III run	I run	II run	III run	I run	II run	III run
Pd/TiO_2	136	139	142	150	154	157	158	163	166
Pd/CeO_2	162	162	166	189	190	192	213	214	217
Pd/Al_2O_3	149	152	155	160	164	170	172	175	182
Pd/Ce/Al_2O_3	141	144	148	150	153	159	161	164	169
Pd/Fe/Al_2O_3	142	145	153	154	157	165	170	172	174
Pd/Mn/Al_2O_3	153	155	159	166	169	175	180	183	189
Pd/Ti/Al_2O_3	150	152	158	163	166	170	183	186	187

[1] Light-off temperatures at 20%, 50% and 80% of propene conversion, respectively.

Table 5. Arrhenius parameters [a], activation energy (E_{act}) and pre-exponential factor A (s^{-1}) of the Pd-supported catalysts.

Catalysts	E_{act} (KJ·mol^{-1})	LnA
Pd/CeO_2	93.7	26.7
Pd/Al_2O_3	132	38.4
Pd/TiO_2	95.3	28.7
Pd/Ce/Al_2O_3	162.6	48.1
Pd/Fe/Al_2O_3	161.1	47.4
Pd/Ti/Al_2O_3	135.1	39.1
Pd/Mn/Al_2O_3	130.7	37.6

[a] E_{act} and A calculated from the Arrhenius plot in the temperature range 100–170 °C.

3. Experimental Section

3.1. Catalyst Preparation

Commercial oxides, CeO_2 (Aldrich, Milano, Italy), γ-Al_2O_3 (Aldrich) and TiO_2 (Euro Support Manufacturing B.V., AMERSFOORT, The Netherlands) were used as supports. The doped alumina oxides, M (5 mol%)/Al_2O_3 (95 mol%), were prepared by wet impregnation of commercial Al_2O_3 with the corresponding metal (Ce, Fe, Mn) nitrate water solution ($Ce(NO_3)_3 \cdot 6H_2O$, $Fe(NO_3)_3 \cdot H_2O$, $Mn(NO_3)_2 \cdot xH_2O$, respectively) or by grafting with $Ti(iso\text{-}OC_3H_7)_4$, then filtered, dried at 120 °C overnight and calcined at 500 °C for 3 h. Pd catalysts were prepared over the above supports by the impregnation method with $Pd(NO_3)_2 \cdot xH_2O$. Then, the obtained powders were calcined at 400 °C for 4 h.

3.2. Catalysts Characterization

The real palladium loading in the catalysts was quantified by ICP-OES Activa (Horiba Jobin-Yvon, Palaiseau, France).

N_2 adsorption-desorption at −196 °C was performed on a Sorptomatic 1900 (Carlo Erba, Trezzano sul Naviglio, Italy) instrument. Before the measurement, the samples were degassed at 300 °C for 3 h. The specific surface area (SSA) of each sample was obtained by the Brunauer–Emmett–Teller (BET) method. The mean pore size diameter was calculated by the Brunauer, Emmet, and Teller (BJH) method applied to the desorption curve.

Powder X-ray diffraction (XRD) patterns were recorded on a Bruker (Milano, Italy) D5005 diffractometer equipped with a Cu-Kα radiation (λ = 1.5418 Å) and a graphite monochromator on the diffracted beam, and the XRD data were generally collected in the 2θ range of 4°–80° with a scanning step size of 0.02° and 0.5 s. The instrumental broadening was determined by collecting the diffraction pattern of the standard, lanthanum hexaboride, LaB_6. The mean crystallite size (d_s) of CeO_2 was calculated with a precision of ±10% from the line broadening of the most intense reflections using the Scherrer Equation (1):

$$d_s = \frac{k \cdot \lambda}{\beta \cdot \cos(\vartheta)} \quad (1)$$

where d_s is the mean size of the ordered (crystalline) domains, which may be smaller or equal to the grain size, k (0.9) is the shape factor, λ (1.54 Å) is the X-ray wavelength, β is the line broadening at half the maximum intensity (FWHM) in radians and θ is the Bragg angle. A corundum probe (Bruker, Milano, Italy) of known crystallinity has been used as the internal standard.

Temperature-programmed reduction/oxidation (TPR/TPO) experiments were carried out with a Micromeritics Autochem 2910 apparatus equipped with a thermal conductivity detector (TCD). TPR experiments were carried out with a flow rate of 50 mL·min^{-1}. The gas mixture with composition 5 vol% H_2 in Ar was used to reduce the catalysts (100 mg). Firstly, the sample was cooled down to −60 °C in a cold trap, and the TCD signal was registered by gradually increasing the temperature (rate 5 °C/min) from −60 °C up to room temperature. After that, the temperature was raised up to 1000 °C at the rate of 10 °C·min^{-1}. Before the TPR was started, the catalysts were pretreated with a flowing gas mixture of 5% O_2 in He (50 mL·min^{-1}) at 120 °C for 1 h in order to purge the surface, then cooling down under Ar. The re-oxidation properties of the catalysts were measured by the TPO experiments. The oxidation gas of 5 vol% O_2 in He (50 mL·min^{-1}) was used to oxidize the catalysts (100 mg), increasing the temperature from room temperature to 1000 °C at a heating rate of 10 °C/min and then decreasing the temperature from 1000 to 100 °C at a cooling rate of 10 °C·min^{-1}.

Chemical states of the atoms in the catalyst surface were investigated by X-ray photoelectron spectroscopy (XPS) on an AXIS Ultra DLD spectrometer marketed by Kratos Analytical, operating with Al (Ka) radiation. XPS data were calibrated using the binding energy of C1s (284.6 eV) as the standard.

High-resolution transmission electron microscopy (HRTEM) analyses were carried out using a JEOL 2100 LaB6 equipped with an Oxford Instruments Inca energy dispersive X-ray (EDX) spectrometer. Mean PdO_x particle size, evaluated as the surface-area weighted diameter ($\bar{d}_{PdO_x}$), was computed according to the following Equation (2):

$$\bar{d}_{PdO_x} = \frac{\sum_i n_i d_i^3}{n_i d_i^2} \tag{2}$$

where n_i represents the number of particles with diameter d_i. On average, 50 images for each catalyst have been collected in order to estimate the particle size.

3.3. Catalytic Tests

The catalytic activity measurements of the propene oxidation were carried out in a tubular fixed-bed reactor under the reactive gas mixture containing 1000 ppm of C_3H_6 and 9 vol% O_2 in He. The total gas flow rate was 7.2 Lh^{-1} and the amount of catalyst 0.2 g, equivalent to a GHSV of 35,000 h^{-1}. In a typical experiment, the fresh catalyst (with grain diameters between 50 and 100 μm) was loaded onto a fine-quartz fritted disk, and the reaction temperature was continuously monitored by a thermocouple inserted inside the furnace. Each catalytic run was performed as follows: introduction of the reaction mixture at room temperature, heating at a rate of 1 °C·min^{-1} up to the final temperature of 450 °C, then cooling down under the reaction mixture. Three consecutive catalytic cycles in propene catalytic oxidation were performed for each catalyst. The total conversion of propene (X) was defined as in Equation (3):

$$X_{C_3H_6}(\%) = 100 \times \frac{[C_3H_6]_{in} - [C_3H_6]_{out}}{[C_3H_6]_{in}} \quad (3)$$

where $[C_3H_6]_{in}$ and $[C_3H_6]_{out}$ denoted the inlet and outlet concentrations of propene, respectively.

3.4. Analysis of Products

The reactants and products of the propene oxidation were analyzed by gas chromatography, using a dual CTR1 column from Alltech (Porapak and molecular sieve) and a TCD for CO, O_2 and CO_2. A Porapak column and an FID were employed for C_3H_6 detection. The only reaction products were CO_2 and H_2O, and the carbon balance was close to ±5% in all of the catalytic tests.

4. Conclusions

The catalytic oxidation of propene was investigated over Pd-supported catalysts over CeO_2-, TiO_2-, Al_2O_3- and Pd-doped-supported catalysts (M/Al_2O_3 oxides; M = Ce, Ti, Fe, Mn). All catalysts presented well-dispersed PdO_x nanoparticles, as confirmed by XRD and TEM. The obtained results showed that the support used has a strong influence on the oxidation state of palladium species and, as a consequence, on the catalytic activity. Pd/TiO_2 and $Pd/Ce/Al_2O_3$ catalysts were the best performing catalysts, while Pd/CeO_2 was performed poorly. Among the series of Pd/doped alumina catalysts, the addition of Ce and Fe improves the catalytic activity with respect to Pd/Al_2O_3, while no positive effect was played by doping of Ti and Mn. The highest activity of the Pd/TiO_2 was attributed to the presence of highly-dispersed Pd^{2+} species easily reducible at −45 °C (as detected by TPR), as well as to the high capability of this catalyst to reoxidize Pd into PdO, as found by TPO. Conversely, in the Pd/CeO_2 catalyst, the presence of Pd^{4+} species only, interacting too strongly with the support, seems responsible for its low catalytic activity.

The addition of Ce to the Pd/Al_2O_3 catalyst increased the Pd-CeO_2 interaction, which promoted the palladium oxide stabilization and the formation of more active sites for the oxidation reaction. The presence in the small crystallites of ceria of high oxygen vacancies associated with the presence of Ce^{3+} also contributes to enhancing the oxygen mobility and increasing the catalytic activity of the $Pd/Ce/Al_2O_3$, making such a catalyst more active than Pd over bare ceria.

Acknowledgments

The authors gratefully acknowledge the scientific services of Institut de Recherches sur la Catalyse et l'Environnement de Lyon (IRCELYON) and, in particular, Prakash Swamy, Laurence Massin and Luis Cardenas (XPS measurements) for stimulating discussions.

Author Contributions

The work was coordinated by Anne Giroir Fendler and Leonarda Francesca Liotta, who contributed equally to the data interpretation and discussion. The manuscript was written by Sonia Gil, who also contributed to the XPS characterization. Mohamed Ousmane performed the synthesis of catalysts and

textural characterization. Giuseppe Pantaleo carried out the TPR and TPO measurements. Jesus Manuel Garcia-Vargas and Laurance Retailleau performed the TEM analyses and catalytic tests.

Conflicts of Interest

The authors declare no conflict of interest.

References

1. Amann, M.; Lutz, M. The revision of the air quality legislation in the European Union related to ground-level ozone. *J. Hazard. Mater.* **2000**, *78*, 41–62.
2. Liotta, L.F.; Ousmane, M.; Di Carlo, G.; Pantaleo, G.; Deganello, G.; Marcì, G.; Retailleau, L.; Giroir-Fendler, A. Total oxidation of propene at low temperature over Co_3O_4–CeO_2 mixed oxides: Role of surface oxygen vacancies and bulk oxygen mobility in the catalytic activity. *Appl. Catal. A* **2008**, *347*, 81–88.
3. Pérez, A.; Molina, R.; Moreno, S. Enhanced voc oxidation over Ce/CoMgAl mixed oxides using a reconstruction method with edta precursors. *Appl. Catal. A* **2014**, *477*, 109–116.
4. Lahousse, C.; Bernier, A.; Grange, P.; Delmon, B.; Papaefthimiou, P.; Ioannides, T.; Verykios, X. Evaluation of γ-MnO_2 as a VOC removal catalyst: Comparison with a noble metal catalyst. *J. Catal.* **1998**, *178*, 214–225.
5. Cloirec, P.L. *Les Composés Organiques Volatils Dans L'environnement*; Lavoisier, Tec et Doc: Paris, France 1998.
6. Hosseini, M.; Barakat, T.; Cousin, R.; Aboukaïs, A.; Su, B.L.; De Weireld, G.; Siffert, S. Catalytic performance of core-shell and alloy Pd-Au nanoparticles for total oxidation of VOC: The effect of metal deposition. *Appl. Catal. B* **2012**, *111–112*, 218–224.
7. Derwent, R.G.; Jenkin, M.E.; Saunders, S.M.; Pilling, M.J. Photochemical ozone creation potentials for organic compounds in northwest europe calculated with a master chemical mechanism. *Atmos. Environ.* **1998**, *32*, 2429–2441.
8. Thevenin, P.O.; Ersson, A.G.; Kušar, H.; Menon, P.; Järås, S.G. Deactivation of high temperature combustion catalysts. *Appl. Catal. A* **2001**, *212*, 189–197.
9. Williamson, W.B.; Lewis, D.; Perry, J.; Gandhi, H.S. Durability of palladium automotive catalysts: Effects of trace lead levels, exhaust composition, and misfueling. *Ind. Eng. Chem. Prod. Res. Dev.* **1984**, *23*, 531–536.
10. Cowley, A. *Platinum 2013. Interim Review*; Johnson Matthey: Hertfordshire, UK, 2013.
11. Okumura, K.; Kobayashi, T.; Tanaka, H.; Niwa, M. Toluene combustion over palladium supported on various metal oxide supports. *Appl. Catal. B* **2003**, *44*, 325–331.
12. Venezia, A.M.; Di Carlo, G.; Liotta, L.F.; Pantaleo, G.; Kantcheva, M. Effect of Ti(IV) loading on CH_4 oxidation activity and SO_2 tolerance of Pd catalysts supported on silica SBA-15 and HMS. *Appl. Catal. B* **2011**, *106*, 529–539.
13. Simplício, L.M.; Brandao, S.T.; Domingos, D.; Bozon-Verduraz, F.; Sales, E.A. Catalytic combustion of methane at high temperatures: Cerium effect on PdO/Al_2O_3 catalysts. *Appl. Catal. A* **2009**, *360*, 2–7.

14. Rooke, J.C.; Barakat, T.; Siffert, S.; Su, B.L. Total catalytic oxidation of toluene using Pd impregnated on hierarchically porous Nb_2O_5 and Ta_2O_5 supports. *Catal. Today* **2012**, *192*, 183–188.
15. Sanchez, M.G.; Gazquez, J.L. Oxygen vacancy model in strong metal-support interaction. *J. Catal.* **1987**, *104*, 120–135.
16. Hong, J.; Chu, W.; Chen, M.; Wang, X.; Zhang, T. Preparation of novel titania supported palladium catalysts for selective hydrogenation of acetylene to ethylene. *Catal. Commun.* **2007**, *8*, 593–597.
17. Marécot, P.; Fakche, A.; Kellali, B.; Mabilon, G.; Prigent, P.; Barbier, J. Propane and propene oxidation over platinum and palladium on alumina: Effects of chloride and water. *Appl. Catal. B* **1994**, *3*, 283–294.
18. Maillet, T.; Solleau, C.; Barbier, J.; Duprez, D. Oxidation of carbon monoxide, propene, propane and methane over a Pd/Al_2O_3 catalyst. Effect of the chemical state of pd. *Appl. Catal. B* **1997**, *14*, 85–95.
19. Ivanova, A.; Korneeva, E.; Slavinskaya, E.; Zyuzin, D.; Moroz, E.; Danilova, I.; Gulyaev, R.; Boronin, A.; Stonkus, O.; Zaikovskii, V. Role of the support in the formation of the properties of a Pd/Al_2O_3 catalyst for the low-temperature oxidation of carbon monoxide. *Kinet. Catal.* **2014**, *55*, 748–762.
20. Chen, X.; Cheng, Y.; Seo, C.Y.; Schwank, J.W.; McCabe, R.W. Aging, re-dispersion, and catalytic oxidation characteristics of model Pd/Al_2O_3 automotive three-way catalysts. *Appl. Catal. B* **2015**, *163*, 499–509.
21. Del Angel, G.; Padilla, J.; Cuauhtemoc, I.; Navarrete, J. Toluene combustion on γ-Al_2O_3-CeO_2 catalysts prepared from boehmite and cerium nitrate. *J. Mol. Catal. A* **2008**, *281*, 173–178.
22. Saitzek, S.; Blach, J.F.; Villain, S.; Gavarri, J.R. Nanostructured ceria: A comparative study from X-ray diffraction, raman spectroscopy and bet specific surface measurements. *Phys. Status Solidi (a)* **2008**, *205*, 1534–1539.
23. Yue, B.; Zhou, R.; Wang, Y.; Zheng, X. Study of the methane combustion and TPR/TPO properties of Pd/Ce-Zr-*M*/Al_2O_3 catalysts with *M* = Mg, Ca, Sr, Ba. *J. Mol. Catal. A* **2005**, *238*, 241–249.
24. Persson, K.; Thevenin, P.; Jansson, K.; Agrell, J.; Järås, S.G.; Pettersson, L.J. Preparation of alumina-supported palladium catalysts for complete oxidation of methane. *Appl. Catal. A* **2003**, *249*, 165–174.
25. Groppi, G.; Cristiani, C.; Lietti, L.; Forzatti, P. Study of PdO/Pd transformation over alumina supported catalysts for natural gas combustion. *Stud. Surf. Sci. Catal.* **2000**, *130*, 3801–3806.
26. Tidahy, H.; Siffert, S.; Lamonier, J.-F.; Zhilinskaya, E.; Aboukaïs, A.; Yuan, Z.-Y.; Vantomme, A.; Su, B.-L.; Canet, X.; de Weireld, G. New Pd/hierarchical macro-mesoporous ZrO_2, TiO_2 and ZrO_2-TiO_2 catalysts for vocs total oxidation. *Appl. Catal. A* **2006**, *310*, 61–69.
27. De la Peña O'Shea, V.; Alvarez-Galvan, M.; Fierro, J.; Arias, P. Influence of feed composition on the activity of Mn and $PdMn/Al_2O_3$ catalysts for combustion of formaldehyde/methanol. *Appl. Catal. B* **2005**, *57*, 191–199.
28. Gaya, U.I.; Abdullah, A.H. Heterogeneous photocatalytic degradation of organic contaminants over titanium dioxide: A review of fundamentals, progress and problems. *J. Photochem. Photobiol. C: Photochem. Rev.* **2008**, *9*, 1–12.

29. Huang, H.; Ye, X.; Zhang, L.; Leung, D.Y.C. Mechanistic study on formaldehyde removal over Pd/TiO_2 catalysts: Oxygen transfer and role of water vapor. *Chem. Eng. J.* **2013**, *230*, 73–79.
30. Ihm, S.-K.; Jun, Y.-D.; Kim, D.-C.; Jeong, K.-E. Low-temperature deactivation and oxidation state of $Pd/\gamma\text{-}Al_2O_3$ catalysts for total oxidation of *n*-hexane. *Catal. Today* **2004**, *93*, 149–154.
31. Aznárez, A.; Korili, S.A.; Gil, A. The promoting effect of cerium on the characteristics and catalytic performance of palladium supported on alumina pillared clays for the combustion of propene.
Appl. Catal. A **2014**, *474*, 95–99.
32. Bi, Y.; Lu, G. Catalytic CO oxidation over palladium supported NaZSM-5 catalysts. *Appl. Catal. B* **2003**, *41*, 279–286.
33. Monteiro, R.S.; Dieguez, L.C.; Schmal, M. The role of pd precursors in the oxidation of carbon monoxide over Pd/Al_2O_3 and $Pd/CeO_2/Al_2O_3$ catalysts. *Catal. Today* **2001**, *65*, 77–89.
34. Ousmane, M.; Liotta, L.F.; di Carlo, G.; Pantaleo, G.; Venezia, A.; Deganello, G.; Retailleau, L.; Boreave, A.; Giroir-Fendler, A. Supported au catalysts for low-temperature abatement of propene and toluene, as model VOCs: Support effect. *Appl. Catal. B* **2011**, *101*, 629–637.
35. Pfau, A.; Schierbaum, K. The electronic structure of stoichiometric and reduced CeO_2 surfaces: An XPS, UPS and HREELS study. *Surf. Sci.* **1994**, *321*, 71–80.
36. Burroughs, P.; Hamnett, A.; Orchard, A.F.; Thornton, G. Satellite structure in the X-Ray Photoelectron Spectra of some binary and mixed oxides of lanthanum and cerium. *J. Chem. Soc. Dalton Trans.* **1976**, 1686–1698.
37. Grosvenor, A.P.; Kobe, B.A.; Biesinger, M.C.; McIntyre, N.S. Investigation of multiplet splitting of Fe 2p XPS spectra and bonding in iron compounds. *Surf. Interface Anal.* **2004**, *36*, 1564–1574.
38. Ferrandon, M.; Carnö, J.; Järås, S.; Björnbom, E. Total oxidation catalysts based on manganese or copper oxides and platinum or palladium I: Characterisation. *Appl. Catal. A: Gen.* **1999**, *180*, 141–151.
39. Fujimoto, K.-I.; Ribeiro, F.H.; Avalos-Borja, M.; Iglesia, E. Structure and reactivity of PdO_x/ZrO_2 catalysts for methane oxidation at low temperatures. *J. Catal.* **1998**, *179*, 431–442.
40. Alexopoulos, K.; Reyniers, M.-F.; Marin, G.B. Reaction path analysis of propene selective oxidation over V_2O_5 and V_2O_5/TiO_2. *J. Catal.* **2012**, *295*, 195–206.
41. Zhai, Z.; Bell, A.T. The kinetics of selective oxidation of propene on bismuth vanadium molybdenum oxide catalysts. *J. Catal.* **2013**, *308*, 25–36.
42. Kobayashi, M.; Kanno, T.; Takeda, H.; Fujisaki, S. Reaction pathway design and optimization in heterogeneous catalysis: Ii. Oscillating partial oxidation of propene on Pt/SiO_2 designed by widely varying dispersion. *Appl. Catal. A* **1997**, *151*, 207–221.